Eur. Phys. J. C (2020) 80:1028
https://doi.org/10.1140/epjc/s10052-020-08574-8

THE EUROPEAN PHYSICAL JOURNAL C

Regular Article - Theoretical Physics

Quark and pion condensates at finite isospin density in chiral perturbation theory

Prabal Adhikari[1,2,a], **Jens O. Andersen**[2,b]

[1] Department of Physics, Wellesley College, 106 Central Street, Wellesley, MA 02481, USA
[2] Department of Physics, Norwegian University of Science and Technology, Høgskoleringen 5, 7491 Trondheim, Norway

Received: 8 April 2020 / Accepted: 19 October 2020 / Published online: 6 November 2020

Abstract In this paper, we consider two-flavor QCD at zero temperature and finite isospin chemical potential μ_I using a model-independent analysis within chiral perturbation theory at next-to-leading order. We calculate the effective potential, the chiral condensate and the pion condensate in the pion-condensed phase at both zero and nonzero pionic source. We compare our finite pionic source results for the chiral condensate and the pion condensate with recent (2+1)-flavor lattice QCD results. Agreement with lattice results generally improves as one goes from leading order to next-to-leading order.

1 Introduction

Quantum Chromodynamics (QCD) has a rich phase structure as a function of temperature and quark chemical potentials [1–3]. The phases are characterized by their symmetry and symmetry-breaking properties. The QCD vacuum breaks chiral symmetry, a symmetry which is unbroken at the level of the Lagrangian itself (for massless quarks). The order parameter for chiral symmetry breaking of the QCD vacuum is the chiral condensate,

$$\langle\bar{\psi}\psi\rangle_0, \tag{1}$$

a zero-momentum (spatially homogeneous) state analogous to the energetically favored Cooper pairing due to the attractive phonon interactions in the Bardeen–Cooper–Schrieffer (BCS) theory of superconductivity [4]. The analogy between chiral symmetry breaking and Cooper-pair formation was first pointed out by Nambu and Jona-Lasinio [5], a physical picture that is affirmed by the presence of Goldstone modes, which are the low energy excitations around the chiral symmetry-broken QCD vacuum. The Goldstone modes are the three pions ($\pi^{\pm}, \pi^0$) in QCD, whose symmetries are consistent with Goldstone's theorem [6] assuming the following symmetry breaking pattern

$$SU(N_f)_L \times SU(N_f)_R \to SU(N_f)_V \tag{2}$$

for $N_f = 2$. The symmetry group of the Lagrangian has $2(N_f^2 - 1)$ generators and that of the vacuum has $N_f^2 - 1$ generators, which leads to exactly $N_f^2 - 1$ Goldstone modes.

Surprisingly, while the evidence for chiral symmetry breaking is convincing, the chiral condensate itself is not a physical observable as is evident through the leading-order Gell-Mann–Oakes–Renner (GOR) relation [7], valid at zero temperature and density

$$m_\pi^2 f_\pi^2 = -(m_u + m_d)\langle\bar{\psi}\psi\rangle_0 + \mathcal{O}(m_q^2 f_\pi^2)\,, \tag{3}$$

where m_π is the pion mass, f_π is the pion decay constant, m_u and m_d are the up and down quarks masses respectively and $q = u, d$. The GOR relation shows that only the product of the quark mass and the chiral condensate can be measured indirectly through a measurement of the pion mass m_π and the pion decay constant f_π. Furthermore, in the chiral limit, the pion mass is zero confirming Nambu's physical picture of chiral symmetry breaking.

The strength of chiral symmetry breaking, as measured by the magnitude of the chiral condensate, changes depending on the physical environment. In the presence of a magnetic field particles are largely restricted to moving in the direction of the magnetic field, an effect known as dimensional reduction [8]. This leads to the strengthening of the quark-antiquark pairing in the chiral condensate channel, an effect analogous to the guaranteed presence of bound states for any potential well in one-dimensional quantum mechanics, (i.e. Cooper's theorem). The chiral condensate for the up-

[a] e-mail: prabal.adhikari@wellesley.edu
[b] e-mail: andersen@tf.phys.ntnu.no (corresponding author)

quark-up-antiquark pairing is more enhanced than that of the down-quark-down-antiquark pairing.

On the other hand, thermal fluctuations, due to the presence of a heat bath, have an opposite effect on the strength of the chiral condensate. Lattice calculations show that chiral symmetry is "restored" at a temperature of approximately $T_c^\chi = 155$ MeV [9–13] though strictly speaking the transition is only a crossover. The crossover temperature is defined by the peak of the chiral susceptibility. This temperature is slightly less than the crossover temperature for the deconfinement transition, $T_c^{\rm decon} \approx 170$ MeV. However this temperature difference is observable dependent. In most cases, $T_c^{\rm decon}$ has been determined by the behavior of the Polyakov loop. Recently, it has been defined by the behavior of the quark entropy and in this case the two crossover temperatures agree within errors [13].

A model-independent analysis within next-to-leading order (NLO) chiral perturbation theory (χPT) shows that

$$\frac{\langle\bar\psi\psi\rangle_T}{\langle\bar\psi\psi\rangle_0} = 1 - \frac{\frac{2}{3}\frac{N_f^2-1}{N_f}}{8f_\pi^2}T^2 + \cdots \tag{4}$$

with the chiral condensate decreasing quadratically with temperature (T) assuming $T \ll 4\pi f_\pi$, the regime of validity of χPT, with the coefficient depending on the number of flavors (N_f) [14–16].

Furthermore, the presence of matter can also have an effect on the chiral condensate. For instance, within nucleons, the valence quarks can expel the chiral condensate as has been shown (in a model-independent calculation [17]) using the Feynman–Hellman theorem. The physics is quite intuitive – the gluons that couple quarks or quarks and antiquarks, favor the formation of protons and neutrons when the quark chemical potential is approximately a third of the proton mass (nucleon density at saturation). As more gluons become confined in protons and neutrons, fewer are confined within the chiral condensate leading to its reduction. The deviation from the vacuum value of the chiral condensate $\langle\bar\psi\psi\rangle_0$ at low nuclear densities ρ_N is

$$\frac{\langle\bar\psi\psi\rangle_\rho}{\langle\bar\psi\psi\rangle_0} = 1 - \frac{\sigma_N}{m_\pi^2 f_\pi^2}\rho_N + \cdots, \tag{5}$$

where σ_N is the pion-nucleon sigma term and ρ_N is the nucleon density. We note that $\sigma_N = 59 \pm 7$ MeV and has been determined empirically using modern scattering data and baryon χPT at $\mathcal{O}(p^3)$ [18]. The nucleon density at complete expulsion is

$$\rho_N^\chi \equiv \frac{m_\pi^2 f_\pi^2}{\sigma_N} \sim (110\ {\rm MeV})^3, \tag{6}$$

which is smaller than the scale $(4\pi f_\pi)^3$, well within the regime of validity of χPT [17]. The uncertainty in the saturation density arises largely due to the uncertainty in determining σ_N [18]. In this paper, we focus on the nature of condensates within next-to-leading order, finite isospin χPT, which is the effective field theory of QCD valid at energies much lower than the typical hadronic scales, i.e.

$$\frac{p_\chi}{4\pi f_\pi} \ll 1, \tag{7}$$

where p_χ is a parameter with mass dimension 1. The quantities relevant for this paper include momentum p, the isospin chemical potential μ_I and a pseudoscalar, pionic source j [19].

We will focus not only on the behavior of the chiral condensate but also on the pion condensate

$$\langle\pi^\pm\rangle_{\mu_I}. \tag{8}$$

In the vacuum phase of QCD, i.e. for values of $|\mu_I| \le \mu_I^c \equiv m_\pi$ it vanishes, while for larger values of μ_I, it is nonzero and we enter the pion-condensed phase of QCD. It is further known that pion condensates due to their electromagnetic charge form currents in a superconducting phase when a weak external magnetic field is present [20,21]. For larger magnetic fields, the pion condensate attains a spatially inhomogeneous structure in the form of a single vortex or a triangular vortex lattice similar in nature to the vortex lattice in type-II superconductors [22,23] explained by BCS theory [4].

Chiral perturbation theory at tree-level shows that the decrease in the size of the chiral condensate that occurs due to the formation of pion condensates is exactly compensated for by an increase in the pion condensate. In particular,

$$\langle\bar\psi\psi\rangle_{\mu_I}^2 + \langle\pi^+\rangle_{\mu_I}^2 = \langle\bar\psi\psi\rangle_0^2. \tag{9}$$

At low isospin chemical potentials,

$$\frac{\mu_I - m_\pi}{m_\pi} \ll 1, \tag{10}$$

the behavior of the chiral condensate in the pion-condensed phase relative to the normal vacuum from model-independent and tree-level calculations within χPT [24] is

$$\frac{\langle\bar\psi\psi\rangle_{\mu_I}}{\langle\bar\psi\psi\rangle_0} = 1 - \frac{1}{2m_\pi f_\pi^2}n_I + \cdots \tag{11}$$

where n_I is the tree-level isospin density, which at low densities scales linearly with the isospin chemical potential. It is worth noting that the ratio of the medium to vacuum chiral condensates (due to the expulsion of the chiral condensate

by the formation of the pion condensed phase) is analogous in structure to the ratio found in nucleons due to expulsion of the chiral condensate through the pairing of the valence quarks $\langle qqq\rangle_\rho$.

Recently there have been lattice computations of finite isospin QCD [25], which does not suffer from the fermion sign problem. This is due to the complex phase cancellation between the up and down quarks which have equal and opposite isospin numbers. Lattice QCD shows that the chiral structure of Eq. (9) is not preserved away from the critical isospin chemical potential. This violation is also observed in model-dependent calculations within the Nambu–Jona-Lasinio (NJL) model [27,28]. For a recent review of meson condensation, see Ref. [28].

In this paper, we perform model-independent calculations of the chiral and pion condensates in the pion-condensed phase at next-to-leading order within χPT. This requires the effective potential $V_{\rm eff}$ at NLO in the presence of a pionic source. This part of the calculation turns out to be a generalization of the result obtained in [29].

The paper is organized as follows. In the next section, we briefly discuss the chiral Lagrangian and the ground state in the presence of a nonzero isospin chemical potential. In Sect. 3, we derive the effective potential at next-to-leading order in χPT including a pionic source. In Sect. 4, we calculate the zero-temperature quark and pion condensates at finite μ_I. In Sect. 5, we plot the quark and pion condensates using lattice QCD parameters. At finite pionic source, we compare our results with the available lattice QCD data.

2 χPT Lagrangian

The Lagrangian of massless two-flavor QCD has a local $SU(3)$ gauge symmetry in addition to the global $SU(2)_L \times SU(2)_R \times U(1)_B$ symmetries. For nonzero quark masses in the isospin limit, i.e for $m_u = m_d$, the symmetries are $SU(2)_V \times U(1)_B$. Adding a quark chemical potential μ_q for each quark, the symmetry is $U(1)_{I_3} \times U(1)_B = U(1)_u \times U(1)_d$. In the pion-condensed phase, the $U(1)_{I_3}$ symmetry is broken and one of the mass eigenstates becomes a Goldstone boson, which is a linear combination of both the charge eigenstates ($\pi^\pm$).

Chiral perturbation theory is a low-energy effective theory for QCD based on the symmetries and degrees of freedom [30–33]. In two-flavor QCD, the degrees of freedom are the pions, while for three-flavor QCD we have additionally the charged and neutral kaons as well the eta. In the low-energy expansion of the Lagrangian in χPT, each covariant derivative counts as order p, while a quark mass term counts as order p^2. We begin with the chiral Lagrangian in the isospin limit at $\mathcal{O}(p^2)$

$$\mathcal{L}_2 = \frac{f^2}{4}\mathrm{Tr}\left[\nabla_\mu \Sigma^\dagger \nabla^\mu \Sigma\right] + \frac{f^2}{4}\mathrm{Tr}\left[\chi^\dagger \Sigma + \Sigma^\dagger \chi\right], \tag{12}$$

where Σ parameterizes the Goldstone boson manifold (see Eqs. (18)–(22) below), f is the bare pion decay constant,

$$\chi = 2B_0 M + 2iB_0 j_1 \tau_1 + 2iB_0 j_2 \tau_2, \tag{13}$$

where $M = \mathrm{diag}(m, m)$ is the quark mass matrix and $-f^2 B_0$ is the tree-level quark condensate. We have introduced a pionic source in χ, which is necessary for calculating the pion condensate. τ_a represent the Pauli matrices and the covariant derivatives are defined as

$$\nabla_\mu \Sigma \equiv \partial_\mu \Sigma - i\left[v_\mu, \Sigma\right], \tag{14}$$

$$\nabla_\mu \Sigma^\dagger = \partial_\mu \Sigma^\dagger - i[v_\mu, \Sigma^\dagger], \tag{15}$$

with

$$\begin{aligned} v_\mu &= \delta_{\mu 0}\mathrm{diag}(\mu_u, \mu_d) \\ &= \delta_{\mu 0}\mathrm{diag}\left(\frac{1}{3}\mu_B + \frac{1}{2}\mu_I, \frac{1}{3}\mu_B - \frac{1}{2}\mu_I\right), \end{aligned} \tag{16}$$

where $\mu_I = \mu_u - \mu_d$ is the isospin chemical potential and $\mu_B = \frac{3}{2}(\mu_u + \mu_d)$ is the baryon chemical potential. We also set $\mu_B = 0$ for the purpose of this paper.[1]

In the two-flavor case, the ground state in χPT is parametrized as [24]

$$\Sigma_\alpha = e^{i\alpha(\hat\phi_1\tau_1 + \hat\phi_2\tau_2)} = \mathbb{1}\cos\alpha + i(\hat\phi_1\tau_1 + \hat\phi_2\tau_2)\sin\alpha, \tag{17}$$

where α at tree level can be interpreted as a rotation angle and $\hat\phi_1^2 + \hat\phi_2^2 = 1$ to ensure the normalization of the ground state, i.e. $\Sigma_\alpha^\dagger \Sigma_\alpha = \mathbb{1}$. In the remainder of the paper we choose $\hat\phi_1 = 1$ and $\hat\phi_2 = 0$, without loss of generality. There will be no reference to j_2 in this case and we write $j_1 = j$ in the remainder. The matrix τ_1 generates the rotations and we can write the rotated vacuum as $\Sigma_\alpha = A_\alpha \Sigma_0 A_\alpha$, where $A_\alpha = e^{i\frac{\alpha}{2}\tau_1}$ and $\Sigma_0 = \mathbb{1}$ is the trivial vacuum.

We also need to parametrize the fluctuations around the condensed vacuum, which requires some care. Since the vacuum is rotated, we must also rotate the generators of the fluctuations in the same manner. This was discussed in Ref. [34] and an explicit example was given in Ref. [29]. The field Σ is written as

$$\Sigma = L_\alpha \Sigma_\alpha R_\alpha^\dagger, \tag{18}$$

with

$$L_\alpha = A_\alpha U A_\alpha^\dagger, \tag{19}$$

$$R_\alpha = A_\alpha^\dagger U^\dagger A_\alpha. \tag{20}$$

[1] In the pion-condensed phase, physical quantities are independent of μ_B [35,36].

Here U is the $SU(2)$ matrix that parametrizes the fluctuations around the ground state $\Sigma_0 = \mathbb{1}$

$$U = e^{i\frac{\phi_a \tau_a}{2f}}. \tag{21}$$

Combining Eqs. (18)–(20), the expression for Σ is

$$\Sigma = A_\alpha (U \Sigma_0 U) A_\alpha = A_\alpha U^2 A_\alpha, \tag{22}$$

which reduces to $\Sigma = U^2$ for $\alpha = 0$ as required.

In order to calculate the effective potential and the condensates to NLO, we need to evaluate the path integral in the Gaussian approximation. In order to do so, we must expand the Lagrangian $\mathcal{L}_2$ in the fields ϕ_a as

$$\mathcal{L}_2 = \mathcal{L}_2^{\text{static}} + \mathcal{L}_2^{\text{linear}} + \mathcal{L}_2^{\text{quadratic}} + \cdots, \tag{23}$$

where the terms we need are

$$\mathcal{L}_2^{\text{static}} = 2f^2 B_0 m_j + \frac{1}{2} f^2 \mu_I^2 \sin^2\alpha, \tag{24}$$

$$\mathcal{L}_2^{\text{linear}} = f\left(-2B_0 \bar{m}_j + \mu_I^2 \sin\alpha\cos\alpha\right)\phi_1 + f\mu_I \sin\alpha \partial_0 \phi_2, \tag{25}$$

$$\mathcal{L}_2^{\text{quadratic}} = \frac{1}{2}\partial_\mu \phi_a \partial^\mu \phi_a - \frac{1}{2} m_a^2 \phi_a^2 + \mu_I \cos\alpha(\phi_1 \partial_0 \phi_2 - \phi_2 \partial_0 \phi_1) \tag{26}$$

and the source-dependent masses are

$$m_j = m\cos\alpha + j\sin\alpha, \tag{27}$$

$$\bar{m}_j = m\sin\alpha - j\cos\alpha, \tag{28}$$

$$m_1^2 = 2B_0 m_j - \mu_I^2 \cos 2\alpha, \tag{29}$$

$$m_2^2 = 2B_0 m_j - \mu_I^2 \cos^2\alpha, \tag{30}$$

$$m_3^2 = 2B_0 m_j + \mu_I^2 \sin^2\alpha. \tag{31}$$

The Lagrangian up to quadratic order reduces to that of Ref. [29] by setting $j = 0$. We get for the inverse propagator:

$$D^{-1} = \begin{pmatrix} D_{12}^{-1} & 0 \\ 0 & P^2 - m_3^2 \end{pmatrix}, \tag{32}$$

where $P = (p_0, p)$, $P^2 = p_0^2 - p^2$, and the 2×2 submatrix is given by

$$D_{12}^{-1} = \begin{pmatrix} P^2 - m_1^2 & ip_0 m_{12} \\ -ip_0 m_{12} & P^2 - m_2^2 \end{pmatrix}. \tag{33}$$

Here the off-diagonal mass is defined as

$$m_{12} = 2\mu_I \cos\alpha. \tag{34}$$

At next-to-leading order in the low-energy expansion, there are ten different operators in the Lagrangian [31]. The terms relevant for the present calculations are [14]

$$\mathcal{L}_4 = \frac{1}{4} l_1 \left(\text{Tr}\left[\nabla_\mu \Sigma^\dagger D^\mu \Sigma\right]\right)^2 + \frac{1}{4} l_2 \text{Tr}\left[\nabla_\mu \Sigma^\dagger D_\nu \Sigma\right] \text{Tr}\left[D^\mu \Sigma^\dagger D^\nu \Sigma\right] + \frac{1}{16}(l_3 + l_4)(\text{Tr}[\chi^\dagger \Sigma + \Sigma^\dagger \chi])^2 + \frac{1}{8} l_4 \text{Tr}\left[\nabla_\mu \Sigma^\dagger D^\mu \Sigma\right] \text{Tr}[\chi^\dagger \Sigma + \Sigma^\dagger \chi] + \frac{1}{2} h_1 \text{Tr}[\chi^\dagger \chi]. \tag{35}$$

Here l_i and h_i are bare couplings. The relations between the bare and renormalized couplings $l_i^r(\Lambda)$ and $h_i^r(\Lambda)$ are [32]

$$l_i = l_i^r(\Lambda) - \frac{\gamma_i \Lambda^{-2\epsilon}}{2(4\pi)^2}\left[\frac{1}{\epsilon} + 1\right], \tag{36}$$

$$h_i = h_i^r(\Lambda) - \frac{\delta_i \Lambda^{-2\epsilon}}{2(4\pi)^2}\left[\frac{1}{\epsilon} + 1\right], \tag{37}$$

where Λ is the renormalization scale in the modified minimal subtraction ($\overline{\text{MS}}$) scheme. The constants γ_i and δ_i are [32]

$$\gamma_1 = \frac{1}{3}, \qquad \gamma_2 = \frac{2}{3}, \qquad \gamma_3 = -\frac{1}{2}, \tag{38}$$

$$\gamma_4 = 2, \qquad \delta_1 = 0. \tag{39}$$

Taking the derivative of Eqs. (36)–(37) with respect to Λ and using that the bare couplings are independent of the scale, one finds that the running couplings satisfy the equations,

$$\Lambda \frac{d}{d\Lambda} l_i^r = -\frac{\gamma_i}{(4\pi)^2}, \tag{40}$$

$$\Lambda \frac{d}{d\Lambda} h_i^r = -\frac{\delta_i}{(4\pi)^2}. \tag{41}$$

These equations can be easily solved for the running couplings l_i^r and h_i^r, The relations between the running couplings and the so-called low-energy constants $\bar{l}_i$ and $\bar{h}_i$ in two-flavor χPT are

$$l_i^r(\Lambda) = \frac{\gamma_i}{2(4\pi)^2}\left[\bar{l}_i + \log\frac{M^2}{\Lambda^2}\right], \tag{42}$$

$$h_i^r(\Lambda) = \frac{\delta_i}{2(4\pi)^2}\left[\bar{h}_i + \log\frac{M^2}{\Lambda^2}\right]. \tag{43}$$

Up to a prefactor, the low-energy constants are the running couplings evaluated at the scale $\Lambda^2 = M^2$. We return to this in the Sect. 5. Note that, due to $\delta_1 = 0$, Eq. (43) does not apply and Eq. (41) shows that $h_1^r(\Lambda)$ does not run. Moreover, in the original paper [31], the authors used another set of invariant operators than the ones (partially) listed in Eq. (35). Using the equations of motion one can obtain one from the other. This implies relations among couplings, $h_1 = \tilde{h}_1 - \tilde{l}_4$, where $\tilde{l}_i$ and $\tilde{h}_i$ refer to the original couplings from Ref. [31]. The corresponding values of $\tilde{\gamma}_i$ and $\tilde{\delta}_i$ are the same as above, except $\tilde{\delta}_1 = 2$ implying that $\tilde{h}_1$ runs.

3 Effective potential

Since the terms $\mathcal{L}_2^{\text{static}}$, $\mathcal{L}_2^{\text{linear}}$, and $\mathcal{L}_2^{\text{quadratic}}$ as well as $\mathcal{L}_4^{\text{static}}$ (see below) can be obtained from the results in Ref. [29] by using source-dependent mass parameters, the calculation of the effective potential here is a straightforward generalization of the calculation therein. However, for completeness, we include the details here. At tree level, the effective potential V_0 is given by $-\mathcal{L}_2^{\text{static}}$,

$$V_0 = -2f^2 B_0 m_j - \frac{1}{2} f^2 \mu_I^2 \sin^2\alpha. \tag{44}$$

The value of α that minimizes the tree-level potential V_0 is given by $\frac{\partial V_0}{\partial \alpha} = 0$ or $2B_0\bar{m}_j - \mu_I^2 \sin\alpha\cos\alpha = 0$. The linear term $\mathcal{L}_2^{\text{linear}}$ in Eq. (25) then vanishes at the minimum of the tree-level potential, as required. (The surface term, $f\mu_I \sin\alpha\partial_0\phi_2$, can be ignored.) At next-to-leading order, there are two contributions to the effective potential, namely the static term $V_1^{\text{static}} = -\mathcal{L}_4^{\text{static}}$ and the one-loop contribution V_1 arising from the Gaussian path integral involving the quadratic terms in the Lagrangian, $\mathcal{L}_2$, given by Eq. (26).

The static part of the NLO effective potential is

$$\begin{aligned} V_1^{\text{static}} = &-(l_1+l_2)\mu_I^4 \sin^4\alpha - 2l_4 B_0 m_j \mu_I^2 \sin^2\alpha \\ &-4(l_3+l_4)B_0^2 m_j^2 - 4h_1 B_0^2[m_j^2 + \bar{m}_j^2], \end{aligned} \tag{45}$$

which acts as counterterms in the NLO calculation.

After performing the Gaussian integral to obtain the one-loop correction, V_1, to the effective potential, we Wick rotate to Euclidean space. The one-loop contribution to the effective potential in Euclidean space of a free massive boson is given by

$$V_1 = \frac{1}{2}\int_P \log[P^2 + m^2], \tag{46}$$

where now $P^2 = p_0^2 + p^2$ and the integral is defined as

$$\int_P = \int \frac{dp_0}{2\pi}\int_p = \int \frac{dp_0}{2\pi}\left(\frac{e^{\gamma_E}\Lambda^2}{4\pi}\right)^{\epsilon}\int \frac{d^d p}{(2\pi)^d}. \tag{47}$$

We use dimensional regularization to regulate ultraviolet divergences with the momentum integral generalized to $d = 3 - 2\epsilon$ dimensions. Then the integral in Eq. (46) becomes

$$\begin{aligned} \int_P \log[P^2 + m^2] &= \int_p \sqrt{p^2 + m^2} \\ &= -\frac{m^4}{2(4\pi)^2}\left(\frac{\Lambda^2}{m^2}\right)^{\epsilon}\left[\frac{1}{\epsilon} + \frac{3}{2} + \mathcal{O}(\epsilon)\right]. \end{aligned} \tag{48}$$

The contribution from π^0 can be calculated analytically in dimensional regularization using Eq. (48),

$$V_{1,\pi^0} = \frac{1}{2}\int_P \log\left[P^2 + m_3^2\right]. \tag{49}$$

The contribution from the charged pions requires a little more work. Using Eq. (48), we obtain

$$\begin{aligned} V_{1,\pi^+} + V_{1,\pi^-} &= \frac{1}{2}\int_P \log[(p_0^2 + E_{\pi^+}^2)(p_0^2 + E_{\pi^-}^2)] \\ &= \frac{1}{2}\int_p \left[E_{\pi^+} + E_{\pi^-}\right], \end{aligned} \tag{50}$$

where the energies $E_{\pi^\pm}$ are found by calculating the zeros of the inverse propagator D_{12}^{-1} and read

$$\begin{aligned} E_{\pi^\pm}^2 = p^2 &+ \frac{1}{2}(m_1^2 + m_2^2 + m_{12}^2) \\ &\pm \frac{1}{2}\sqrt{4p^2 m_{12}^2 + (m_1^2 + m_2^2 + m_{12}^2)^2 - 4m_1^2 m_2^2}. \end{aligned} \tag{51}$$

In order to eliminate the divergences, their dispersion relations are expanded in powers of $1/p$ as

$$\begin{aligned} E_{\pi^+} + E_{\pi^-} = 2p &+ \frac{2(m_1^2 + m_2^2) + m_{12}^2}{4p} \\ &- \frac{8(m_1^4 + m_2^4) + 4(m_1^2 + m_2^2)m_{12}^2 + m_{12}^4}{64p^3} \\ &+ \cdots \end{aligned} \tag{52}$$

To this order, the large-p behavior in Eq. (52) is the same as the sum $E_1 + E_2$, where the energies and masses are $E_{1,2} = \sqrt{p^2 + m_{1,2}^2 + \frac{1}{4}m_{12}^2} = \sqrt{p^2 + \tilde{m}_{1,2}^2}$, $\tilde{m}_1^2 = m_3^2$ and $\tilde{m}_2^2 = 2B_0 m_j$. We can then write

$$V_{1,\pi^+} + V_{1,\pi^-} = V_{1,\pi^+}^{\text{div}} + V_{1,\pi^-}^{\text{div}} + V_{1,\pi^+}^{\text{fin}} + V_{1,\pi^-}^{\text{fin}}, \tag{53}$$

where

$$V_{1,\pi^+}^{\text{div}} + V_{1,\pi^-}^{\text{div}} = \frac{1}{2}\int_p [E_1 + E_2], \tag{54}$$

$$V_{1,\pi^+}^{\text{fin}} + V_{1,\pi^-}^{\text{fin}} = \frac{1}{2}\int_p \left[E_{\pi^+} + E_{\pi^-} - E_1 - E_2\right]. \tag{55}$$

The divergent integrals in Eq. (54) can be done analytically in dimensional regularization. The subtraction integral (55) is finite and can be computed numerically.

Using Eq. (48), the divergent part of the one-loop contribution can be written as

$$\begin{aligned} V_1^{\text{div}} &= V_{1,\pi^0} + V_{1,\pi^+}^{\text{div}} + V_{1,\pi^-}^{\text{div}} \\ &= -\frac{\tilde{m}_1^4}{4(4\pi)^2}\left[\frac{1}{\epsilon} + \frac{3}{2} + \log\left(\frac{\Lambda^2}{\tilde{m}_1^2}\right)\right] \\ &\quad -\frac{\tilde{m}_2^4}{4(4\pi)^2}\left[\frac{1}{\epsilon} + \frac{3}{2} + \log\left(\frac{\Lambda^2}{\tilde{m}_2^2}\right)\right] \\ &\quad -\frac{m_3^4}{4(4\pi)^2}\left[\frac{1}{\epsilon} + \frac{3}{2} + \log\left(\frac{\Lambda^2}{m_3^2}\right)\right]. \end{aligned} \tag{56}$$

Renormalization is now carried out by adding Eqs. (44), (45), and (56), using Eqs. (36)–(37). Using Eq. (42), the renormal-

ized effective potential is

$$
\begin{aligned}
V_{\text{eff}} = &-2f^2B_0m_j - \frac{1}{2}f^2\mu_I^2\sin^2\alpha \\
&-\frac{1}{(4\pi)^2}\left[\frac{3}{2} - \bar{l}_3 + 4\bar{l}_4 + \log\left(\frac{M^2}{\tilde{m}_2^2}\right)\right. \\
&\left.+2\log\left(\frac{M^2}{m_3^2}\right)\right]B_0^2m_j^2 \\
&-\frac{1}{(4\pi)^2}\left[\frac{1}{2} + \bar{l}_4 + \log\left(\frac{M^2}{m_3^2}\right)\right]2B_0m_j\mu_I^2\sin^2\alpha \\
&-\frac{1}{2(4\pi)^2}\left[\frac{1}{2} + \frac{1}{3}\bar{l}_1 + \frac{2}{3}\bar{l}_2 + \log\left(\frac{M^2}{m_3^2}\right)\right]\mu_I^4\sin^4\alpha \\
&-\frac{4}{(4\pi)^2}\bar{h}_1B_0^2\left[m_j^2 + \bar{m}_j^2\right] + V_{1,\pi^+}^{\text{fin}} + V_{1,\pi^-}^{\text{fin}}. \qquad (57)
\end{aligned}
$$

For zero pionic source, $j = 0$, Eq. (57) reduces to the result of Ref. [29] after subtracting the constant term proportional to $\bar{h}_1$. We note that since h_1^r does not run due to Eq. (41), we have defined $\bar{h}_1 = (4\pi)^2h_1^r = (4\pi)^2h_1$.

4 Quark and pion condensates

In Refs. [29,35,36], we studied the thermodynamic properties of the pion-condensed phase of QCD at $T = 0$ at next-to-leading order by calculating the first quantum correction to the tree-level potential. It was shown that the transition from the vacuum phase to a pion-condensed phase is second order and takes place at a critical isospin chemical potential $\mu_I^c = m_\pi$, where m_π is the physical pion mass. We continue the study of the pion-condensed phase by calculating the quark and pion condensates.

In the isospin limit, the quark condensates $\langle\bar{u}u\rangle$ and $\langle\bar{d}d\rangle$ are equal and in the following we denote each of them by $\langle\bar{\psi}\psi\rangle$. The quark and pion condensates at finite isospin are then defined as [2]

$$
\langle\bar{\psi}\psi\rangle_{\mu_I} = \frac{1}{2}\frac{\partial V_{\text{eff}}}{\partial m}, \qquad \langle\pi^+\rangle_{\mu_I} = \frac{1}{2}\frac{\partial V_{\text{eff}}}{\partial j}. \qquad (58)
$$

At tree level, the condensates are given by the partial derivatives of V_0, which yields

$$
\langle\bar{\psi}\psi\rangle_{\mu_I}^{\text{tree}} = -f^2B_0\cos\alpha = \langle\bar{\psi}\psi\rangle_0^{\text{tree}}\cos\alpha, \qquad (59)
$$

$$
\langle\pi^+\rangle_{\mu_I}^{\text{tree}} = -f^2B_0\sin\alpha = \langle\bar{\psi}\psi\rangle_0^{\text{tree}}\sin\alpha, \qquad (60)
$$

[2] Note that in the finite isospin lattice QCD simulation of Ref. [25], $\langle\bar{\psi}\psi\rangle = \langle\bar{u}u\rangle + \langle\bar{d}d\rangle$ but in our notation $\langle\bar{\psi}\psi\rangle = \langle\bar{u}u\rangle = \langle\bar{d}d\rangle$. Consequently, there is an explicit factor of $\frac{1}{2}$ in our definition of $\langle\bar{\psi}\psi\rangle$. Additionally, compared to Ref. [25], we define the pion condensate with an extra factor of $\frac{1}{2}$. The pionic source λ in Ref. [25] corresponds exactly to j in this paper.

where $\langle\bar{\psi}\psi\rangle_0^{\text{tree}} = -f^2B_0$ denotes the quark condensate in the vacuum phase. Equations (59)–(60) show that we can interpret α as a rotation angle such that the quark condensate is rotated into a pion condensate. As we shall see below, this interpretation is not valid at next-to-leading order and is not seen on the lattice. At next-to-leading order in the low-energy expansion, the quark condensate is

$$
\begin{aligned}
\langle\bar{\psi}\psi\rangle_{\mu_I} = &-f^2B_0\cos\alpha\left[1 + \frac{1}{(4\pi)^2}\left(-\bar{l}_3 + 4\bar{l}_4\right.\right. \\
&\left.+\log\frac{M^2}{\tilde{m}_2^2} + 2\log\frac{M^2}{m_3^2}\right)\frac{B_0m_j}{f^2} \\
&\left.+\frac{1}{(4\pi)^2}\left(\bar{l}_4 + \log\frac{M^2}{m_3^2}\right)\frac{\mu_I^2\sin^2\alpha}{f^2}\right] \\
&-\frac{4}{(4\pi)^2}\bar{h}_1B_0^2m + \frac{1}{2}\frac{\partial V_{1,\pi^+}^{\text{fin}}}{\partial m} + \frac{1}{2}\frac{\partial V_{1,\pi^-}^{\text{fin}}}{\partial m}. \qquad (61)
\end{aligned}
$$

In the limit of vanishing source j and $\alpha = 0$, Eq. (61) is independent of the isospin chemical potential and are consistent with expressions given in Refs. [31,32].

At next-to-leading order in the low-energy expansion, the pion condensate is

$$
\begin{aligned}
\langle\pi^+\rangle_{\mu_I} = &-f^2B_0\sin\alpha\left[1 + \frac{1}{(4\pi)^2}\left(-\bar{l}_3 + 4\bar{l}_4\right.\right. \\
&\left.+\log\frac{M^2}{\tilde{m}_2^2} + 2\log\frac{M^2}{m_3^2}\right)\frac{B_0m_j}{f^2} \\
&\left.+\frac{1}{(4\pi)^2}\left(\bar{l}_4 + \log\frac{M^2}{m_3^2}\right)\frac{\mu_I^2\sin^2\alpha}{f^2}\right] \\
&-\frac{4}{(4\pi)^2}\bar{h}_1B_0^2j + \frac{1}{2}\frac{\partial V_{1,\pi^+}^{\text{fin}}}{\partial j} + \frac{1}{2}\frac{\partial V_{1,\pi^-}^{\text{fin}}}{\partial j}. \qquad (62)
\end{aligned}
$$

We note that the pion condensate vanishes in the normal vacuum since $\alpha = 0$ and such a vacuum only exists if the pion source is zero. However, in the presence of a pionic source, i.e. $j \neq 0$, the pion condensate is non-zero not only due to α-dependent contributions but also a term proportional to j, which is independent of α. The term arises due to the non-dynamical contribution $\frac{1}{2}h_1\text{Tr}[\chi^\dagger\chi]$ in the $\mathcal{O}(p^4)$ χPT Lagrangian.

5 Results and discussion

In this section, we present our numerical results for the chiral condensate and the pion condensate both at zero and non-zero pionic source. We compare the non-zero pionic source results with lattice simulations for which lattice data are available. Finite isospin QCD on the lattice is studied by adding an explicit pionic source since spontaneous symmetry breaking in finite volume is forbidden. Obtaining the chiral and pion condensate then requires not just taking the continuum limit

but also extrapolating to a zero external source, which is technically challenging on the lattice

The quark condensate is given by Eq. (61), while the pion condensate is given by Eq. (62). The value of α in the equations is found by extremizing the effective potential, i.e. solving of Eq. (57), $\frac{\partial V_{\text{eff}}}{\partial \alpha} = 0$.

5.1 Definitions and choice of parameters

The chiral condensate depends on the low-energy constant $\bar{h}_1$ of two-flavor χPT, which is unphysical and undeterminable within χPT [37,38]. Furthermore, $\bar{h}_1$ is scale-independent and does not affect the ground state value of α. Consequently, we define the quark and pion condensate deviations relative to the values of the respective condensates at zero isospin and zero pionic source. The definitions of the condensate deviations [3] are [39]

$$\Sigma_{\bar{\psi}\psi} = -\frac{2m}{m_\pi^2 f_\pi^2}\left[\langle\bar{\psi}\psi\rangle_{\mu_I} - \langle\bar{\psi}\psi\rangle_0^{j=0}\right] + 1, \tag{63}$$

$$\Sigma_\pi = -\frac{2m}{m_\pi^2 f_\pi^2}\langle\pi^+\rangle_{\mu_I}, \tag{64}$$

where m is the degenerate mass of the up and down quarks, m_π is the pion mass, and f_π is the pion decay constant. $\langle O\rangle_{\mu_I}$ is the value of the condensate O at an isospin chemical potential μ_I and a pionic source j. $\langle\bar{\psi}\psi\rangle_0^{j=0}$ is the value of the chiral condensate when $\mu_I = 0$ and $j = 0$. The definition of the chiral condensate deviation, $\Sigma_{\bar{\psi}\psi}$, ensures that it is equal to 1 when $\mu_I = 0$ and $j = 0$ and the definition of the pion condensate deviation does not contain a trivial subtraction of the pion condensate at zero pionic source and zero isospin, $\langle\pi^+\rangle_0^{j=0}$, since it equals zero. Since the pion condensate deviation, Σ_π, is a rescaled, dimensionless quantity proportional to the pion condensate of Eq. (62), it is worth noting again that just like the pion condensate it vanishes in the absence of a pionic source if $\alpha = 0$ but when a pionic source is turned on, the deviation becomes non-zero not only due to α-independent terms but also a term proportional to j that is independent of α. Furthermore, the definitions of the deviations ensure that the following constraint is satisfied at tree level including for any pionic source j

$$\left(\Sigma_{\bar{\psi}\psi}^{\text{tree}}\right)^2 + \left(\Sigma_\pi^{\text{tree}}\right)^2 = 1\,, \tag{65}$$

which is consistent with Eqs. (59) and (60). However the constraint is not satisfied at next-to-leading order as will be evident.

[3] Note that compared to Ref. [25], our definitions of the condensate deviations carry an explicit factor 2, which is exactly compensated by the difference of a factor of $\frac{1}{2}$ each in our definitions of $\langle\bar{\psi}\psi\rangle$ and $\langle\pi^+\rangle$.

For our calculation of the condensate deviations, we choose the following values of the quark masses [40]

$$m_u = 2.15\ \text{MeV}, m_d = 4.79\ \text{MeV}, \tag{66}$$

$$m = \frac{m_u + m_d}{2} = 3.47\ \text{MeV}. \tag{67}$$

Since we want to compare our results to those of recent lattice calculations [41], we choose their values for the pion mass and the pion decay constant,

$$m_\pi = 131 \pm 3\ \text{MeV},\ f_\pi = \frac{128 \pm 3}{\sqrt{2}}\text{MeV}. \tag{68}$$

It is important to point out that the quark masses quoted above from [40] are not the quark masses of [41] (they are not known). The quark masses of [40] correspond to a pion mass of approximately 135 MeV, i.e. approximately 3% higher than the one used in the lattice simulations. In order to improve the overall confidence in our comparison, we therefore vary the quark mass m by 5%, which is consistent with uncertainties quoted in Ref. [40].

The LECs of two-flavor χPT and their respective uncertainties are defined at the scale $\Lambda^2 = 2B_0 m$ through Eq. (43) [42] [4]

$$\bar{l}_1 = -0.4 \pm 0.6, \qquad \bar{l}_2 = 4.3 \pm 0.1, \tag{69}$$

$$\bar{l}_3 = 2.9 \pm 2.4, \qquad \bar{l}_4 = 4.4 \pm 0.2 \tag{70}$$

$$\bar{h}_1 = -1.5 \pm 0.2. \tag{71}$$

The LEC, $\bar{h}_1$, was deduced using the value of H_2^r and its uncertainties in Ref. [37] and the mapping of 3-flavor LECs to 2-flavor LECs discussed in Ref. [32]. The chiral condensate deviation is independent of $\bar{h}_1$ at all values of j but the pion condensate deviation depends on $\bar{h}_1$ at finite j. There is at least another choice of $\bar{h}_1$ in literature [31], which happens to be model-dependent (calculations based on ρ-dominance). However, the pion condensate deviation is not affected significantly by this choice [43]. The physical pion mass m_π and the physical pion decay constant f_π can be calculated within χPT at NLO [31],

$$m_\pi^2 = 2B_0 m\left[1 - \frac{B_0 m}{(4\pi)^2 f^2}\bar{l}_3\right], \tag{72}$$

$$f_\pi^2 = f^2\left[1 + \frac{4B_0 m}{(4\pi)^2 f^2}\bar{l}_4\right]. \tag{73}$$

Given the values m_π, f_π, $\bar{l}_3$, and $\bar{l}_4$, we can calculate the parameters f and $2B_0 m$ appearing in the chiral Lagrangian:

$$m_{\pi,0}^{\text{cen}} = 132.49\,\text{MeV}, \qquad f^{\text{cen}} = 84.93\,\text{MeV}, \tag{74}$$

[4] Note that we take the derivative of V_{eff} w.r.t. the quark mass, m, before we choose the scale $\Lambda^2 = 2B_0 m$.

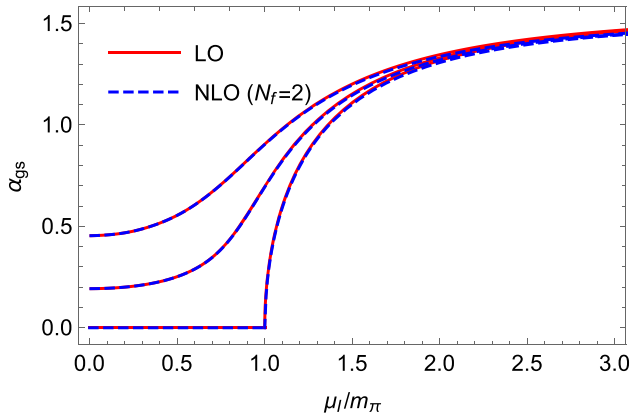

Fig. 1 α_{gs} as a function of μ_I/m_π from below for $j = 0$, $j = 0.00517054 m_\pi$ and $j = 0.0129263 m_\pi$. Red solid lines are LO results and blue dashed lines are NLO results

$$m_{\pi,0}^{\min} = 128.24\,\text{MeV}, \qquad f^{\min} = 83.29\,\text{MeV}, \tag{75}$$

$$m_{\pi,0}^{\max} = 136.91\,\text{MeV}, \qquad f^{\max} = 86.54\,\text{MeV}, \tag{76}$$

where $m_{\pi,0}^2 \equiv 2B_0 m$. Using this relation, we can calculate B_0, which also depends on the tree-level pion mass and the continuum value of the quark mass.

5.2 α_{gs}

Before we discuss the condensates, we present the solution α_{gs} to the equation $\frac{\partial V_{\text{eff}}}{\partial \alpha} = 0$ as function of μ_I/m_π for three different values of the source j. The resulting curves are shown in Fig. 1. The red solid lines are the leading-order results, while the dashed blue lines are the next-to-leading order results. In all three cases, the difference is very small.

For $j = 0$ the curve for α_{gs} is not smooth at $\mu_I = m_\pi$, which simply reflects the second-order transition from the vacuum phase to the pion-condensed phase. For nonzero source, the isospin symmetry is explicitly broken resulting in nonzero values of α_{gs} for all values of μ_I. Moreover, the curves are smooth, which is due to the cross-over nature of the transition, rather than a second-order phase transition. In the limit $\mu_I \to \infty$, the curves approach the asymptotic value of $\alpha_{gs} = \frac{\pi}{2}$.

5.3 Condensates at $j = 0$

In Fig. 2, we plot the $T = 0$ quark condensate deviation (which is normalized to 1) and the pion condensate deviation defined in Eqs. (63) and (64) respectively. In the upper panel of Fig. 2, we plot the tree level chiral condensate deviation in solid red and the next-to-leading order deviation in dashed blue. Similarly, in the bottom panel of Fig. 2, we plot the tree-level pion condensate deviation in solid red and the next-to-leading order deviation in dashed blue. Note that at $j = 0$,

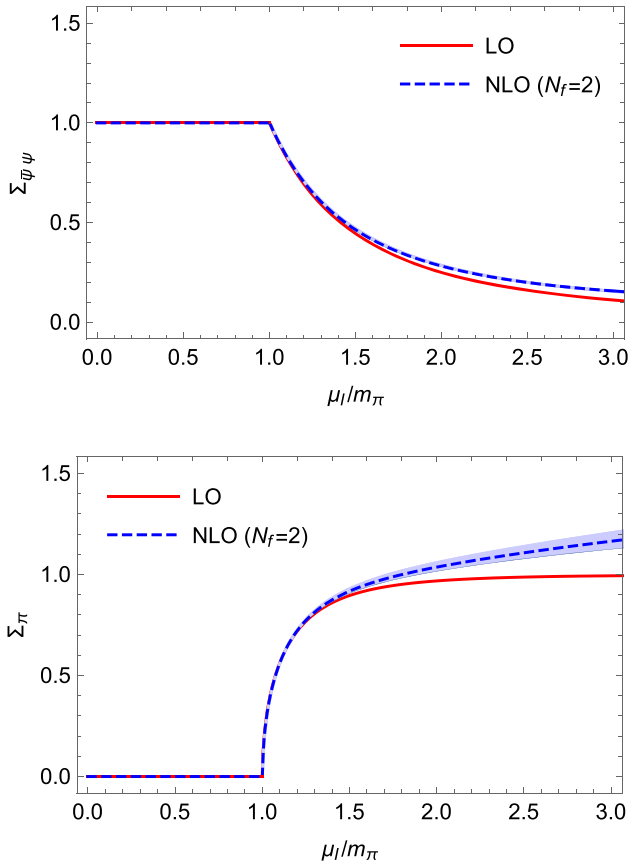

Fig. 2 Top: Quark condensate deviation (normalized to 1) from the normal vacuum value, $\Sigma_{\bar\psi\psi}$, at $T = 0$. Bottom: Pion condensate deviation from the normal vacuum value (which is 0), Σ_π, at $T = 0$ and $j = 0$. See text in Section 5.3 for details

the tree-level deviations are independent of the quark mass. The light blue shaded regions in the two panels of Fig. 2 represent the uncertainty in the condensate deviations due to the uncertainty in the values of the pion mass and the pion decay constant from the lattice, the uncertainty in the LECs, which arises due to experimental uncertainties, and the uncertainty in the lattice quark masses at the 5% level which is consistent with results in Ref. [40]. We note that the uncertainty in the condensate deviations is dominated by the uncertainties in the pion mass and pion decay constant with the uncertainties in the LECs and the quark masses not contributing significantly.

We find that relative to the tree-level condensate deviations, the next-to-leading condensate deviations are moderately larger for the chiral condensate and significantly larger for the pion condensate. The magnitude of the chiral condensate deviation at next-to-leading order decreases more slowly and the magnitude of the pion condensate increases more rapidly compared to their respective tree-level values. Furthermore, the tree-level pion condensate deviation asymp-

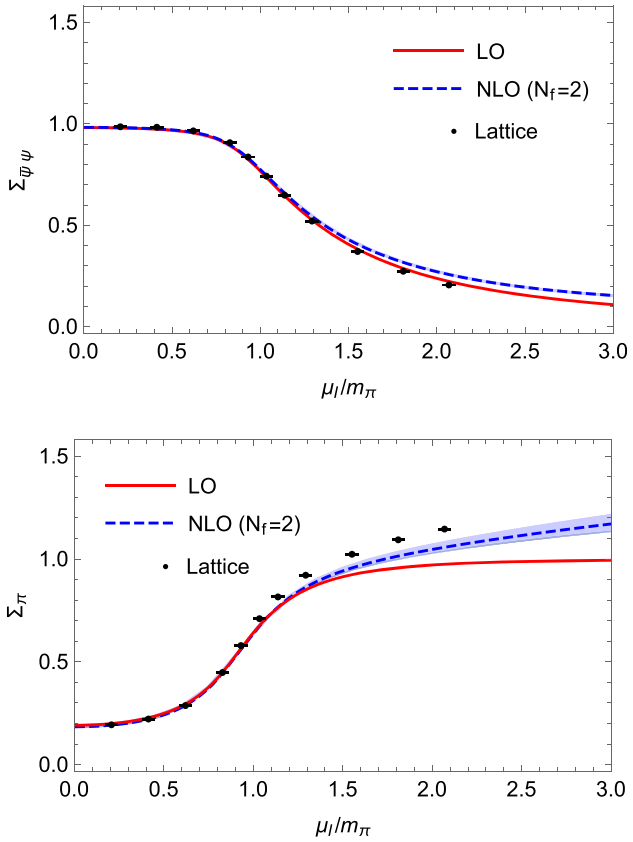

Fig. 3 Top: Quark condensate deviation from the normal vacuum value, $\Sigma_{\bar{\psi}\psi}$, at $T = 0$. Bottom: Pion condensate deviation from the normal vacuum value (which is 0), Σ_π, at $T = 0$ and $j = 0.00517054 m_\pi$. See text in Sect. 5.4 for details

totes to 1 very efficiently, a behavior which is absent at next-to-leading order.

5.4 Condensates at finite j and comparison with lattice QCD

In this section, we plot the chiral and pion condensate deviations at $T = 0$ with a non-zero pionic source ($j \neq 0$) and compare our results with lattice QCD [25,41]. We note that while there is no lattice QCD data available for comparison at $j = 0$, the comparison of finite-j condensate deviations from χPT with the lattice allows us to gauge the quality of our $j = 0$ results calculated at next-to-leading order in χPT. A non-zero j is required to stabilize lattice simulations and consequently $j = 0$ results are "cumbersome" to generate [39].

In Fig. 3, we show the chiral condensate deviation in the top panel and pion condensate deviation in the bottom panel. The deviations are calculated at $j = 0.00517054 m_\pi$, which is the smallest value of the pionic source for which lattice QCD data is available at $T = 0$. In order to perform this comparison fairly, it is important to know the exact quark masses in the continuum since this determines the χPT parameter, B_0, on which the condensates depend. As mentioned above, continuum quark masses have not been calculated in the lattice QCD study. Consequently, in order to make the comparison quantitative we use the lattice continuum quark masses from a separate lattice QCD simulation [40] while incorporating uncertainties at the 5% level which are consistent with the uncertainties quoted. We find that condensate deviations are not very sensitive to the quark masses but most sensitive to the uncertainties in the pion mass and pion decay constants.

We also note that due to the presence of an external pionic source, the ground state explicitly breaks isospin symmetry. Consequently, there is no second order phase transition as there is in the absence of the pionic source. Instead, the transition is a crossover involving a range of isospin chemical potentials within which the chiral and pion condensates change significantly.

The condensate deviations in Fig. 3 show very good agreement with the lattice for isospin chemicals potential up to $\mu_I \approx 1.5 m_\pi$. For larger isospin chemical potentials, the lattice chiral condensate deviation is slightly smaller than the corresponding deviation from χPT at next-to-leading order and the lattice pion condensate deviation is moderately larger than the corresponding deviation from χPT at next-to-leading order. For the quark condensate, the LO result is slightly better than the NLO result for large values of μ_I. For all values of the isospin chemical potential, the next-to-leading order χPT pion condensate deviation is a significant improvement over the tree-level results. In particular, there is qualitatively different behavior for the pion condensate deviation at large isospin chemical potential where the deviation does not level off but increases, which is consistent with the behavior of lattice QCD data. The difference between the tree-level pion condensate deviation and the corresponding lattice QCD deviation is significantly more prominent.

Finally, in Fig. 4, we show the chiral condensate deviation on the top panel and the pion condensate deviation on the bottom panel for $j = 0.0129263 m_\pi$, including χPT results at tree-level, next-to-leading order and lattice QCD including uncertainties. As with the previous figure, the results at next-to-leading order χPT are an improvement over tree level deviations except for the chiral condensate deviation at large isospin chemical potentials for which there is a mild decrease in agreement and for the pion condensate at low isospin chemical potentials, where the decrease in agreement is even milder. The improvement is most significant in the pion condensate deviation, which shows a qualitatively different asymptotic behavior – the next-to-leading order pion condensate deviation does not asymptotically approach 1 as the tree-level result does. The agreement of the deviations with lattice QCD is very good especially for lower values of isospin chemical potential consistent with the fact that χPT is an effective theory with systematic corrections that

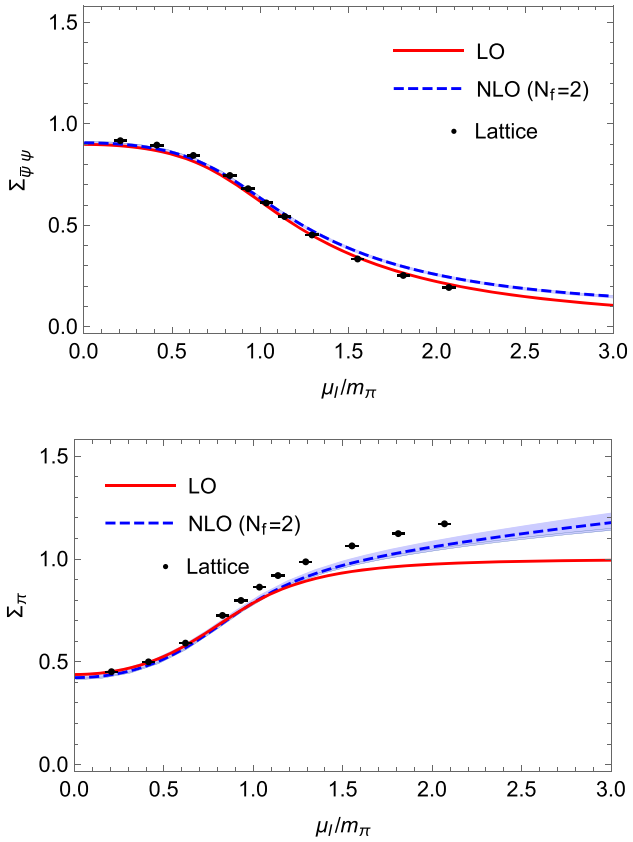

Fig. 4 Top: Quark condensate deviation from the normal vacuum value, $\Sigma_{\bar{\psi}\psi}$, at $T = 0$. Bottom: Pion condensate deviation from the normal vacuum value (which is 0), Σ_π, at $T = 0$ and $j = 0.0129263 m_\pi$. See text in Sect. 5.4 for details

increase with the isospin chemical potential. We also note that the discrepancy between the condensate deviations at larger isospin chemical potentials is larger for $j = 0.0129263 m_\pi$ than $j = 0.00517054 m_\pi$, which is again consistent with expectations for an effective theory. This is a general feature up to the largest values of j used in the simulations.

In conclusion, we have performed a calculation of the quark and pion condensates at next-to-leading order χPT in the absence of an external pionic (pseudoscalar) source for the first time – the results presented here can be used to gauge the quality of future lattice calculation of the chiral and pion condensate at zero source, a calculation that is currently quite challenging to perform. We have also calculated the condensates at finite pionic source and performed a qualitative comparison with the lattice which shows an improved agreement after we include next-to-leading order corrections.

Acknowledgements The authors would like to thank B. Brandt, G. Endrődi and S. Schmalzbauer for providing their lattice condensate data in the presence of a finite pionic source [25]. The authors would also like to acknowledge Martin Mojahed for useful discussions and suggestions.

Data Availability Statement This manuscript has no associated data or the data will not be deposited. [Authors' comment: The plots (excluding the lattice QCD data in Figs. 3 and 4) were generated using the analytical results calculated in this paper. These can be requested from the authors.]

Funded by SCOAP[3].

References

1. K. Rajagopal, F. Wilczek, *At the Frontier of Particle Physics*, vol. 3 (World Scientific, Singapore, 2001), p. 2061
2. M.G. Alford, A. Schmitt, K. Rajagopal, T. Schäfer, Rev. Mod. Phys. **80**, 1455 (2008)
3. K. Fukushima, T. Hatsuda, Rep. Prog. Phys. **74**, 014001 (2011)
4. J. Bardeen, L.N. Cooper, J.R. Schrieffer, Phys. Rev. **106**, 162 (1957)
5. Y. Nambu, G. Jona-Lasinio, Phys. Rev. **122**, 345 (1961)
6. J. Goldstone, A. Salam, S. Weinberg, Phys. Rev. **127**, 965 (1962)
7. M. Gell-Mann, R.J. Oakes, B. Renner, Phys. Rev. **175**, 2195 (1968)
8. G.S. Bali, F. Bruckmann, G. Endrődi, Z. Fodor, S.D. Katz, A. Schäfer, Phys. Rev. D **86**, 071502 (2012)
9. Y. Aoki, Z. Fodor, S. Katz, K. Szabo, Phys. Lett. B **643**, 46 (2006)
10. Y. Aoki, S. Borsanyi, S. Dürr, Z. Fodor, S.D. Katz et al., JHEP **0906**, 088 (2009)
11. S. Borsanyi et al., (Wuppertal-Budapest Collaboration), JHEP **1009**, 073 (2010)
12. A. Bazavov, T. Bhattacharya, M. Cheng, C. DeTar, H. Ding et al., Phys. Rev. D **85**, 054503 (2012)
13. A. Bazavov et al., Phys. Rev. D **93**, 114502 (2016)
14. P. Gerber, H. Leutwyler, Nucl. Phys. B **321**, 387 (1989)
15. V. Koch, Aspects of chiral symmetry. Int. J. Mod. Phys. E **6**, 203 (1997)
16. I.A. Shushpanov, A.V. Smilga, Phys. Lett. B **402**, 351 (1997)
17. T.D. Cohen, R.J. Furnstahl, D.K. Griegel, Phys. Rev. C **45**, 1881 (1992)
18. J.M. Alarcon, J. Martin Camalich, J.A. Oller, Phys. Rev. D **85**, 051503 (2012)
19. S. Scherer, Adv. Nucl. Phys. **27**, 277 (2003)
20. P. Adhikari, T.D. Cohen, J. Sakowitz, Phys. Rev. C **91**, 045202 (2015)
21. P. Adhikari, Phys. Lett. B **790**, 211 (2019)
22. A.A. Abrikosov, Sov. Phys. JETP **5**, 1174 (1957)
23. A.A. Abrikosov, Zh. Eksp, Teor. Fiz. **32**, 1442 (1957)
24. D.T. Son, M.A. Stephanov, Phys. Rev. Lett. **86**, 592 (2001)
25. B.B. Brandt, G. Endrődi, E.S. Fraga, M. Hippert, J. Schaffner-Bielich, S. Schmalzbauer, Phys. Rev. D **98**, 094510 (2018)
26. T. Xia, L. He, P. Zhuang, Phys. Rev. D **88**, 056013 (2013)
27. S.S. Avancini, A. Bandyopadhyay, D.C. Duarte, R.L.S. Farias, Phys. Rev. D **100**, 116002 (2019)
28. M. Mannarelli, Particles **2**, 411 (2019)
29. P. Adhikari, J.O. Andersen, P. Kneshcke, Eur. Phys. J. C **79**, 874 (2019)

30. S. Weinberg, Phys. A **96**, 327 (1979)
31. J. Gasser, H. Leutwyler, Ann. Phys. **158**, 142 (1984)
32. J. Gasser, H. Leutwyler, Nucl. Phys. B **250**, 465 (1985)
33. J. Bijnens, G. Colangelo, G. Ecker, Ann. Phys. **280**, 100 (2000)
34. K. Splittorff, D.T. Son, M.A. Stephanov, Phys. Rev. D **64**, 016003 (2001)
35. P. Adhikari, J.O. Andersen, Phys. Lett. B **804**, 135352 (2020)
36. P. Adhikari, J.O. Andersen, JHEP **06**, 170 (2020)
37. M. Jamin, Phys. Lett. B **538**, 71 (2002)
38. J. Bordes, C.A. Dominguez, P. Moodley, J. Peñarrocha, K. Schilcher, JHEP **10**, 102 (2012)
39. B.B. Brandt, G. Endrődi, S. Schmalzbauer, Phys. Rev. D **97**, 054514 (2018)
40. BMW Collaboration, S. Durr, Z. Fodor, C. Hoelbling, S.D. Katz, S. Krieg, T. Kurth, L. Lellouch, T. Lippert, K.K. Szabo, G. Vulvert, Phys. Lett. B **701**, 265 (2011)
41. G. Endrődi, Private communication
42. G. Colangelo, J. Gasser, H. Leutwyler, Nucl. Phys. B **603**, 125 (2001)
43. M. Mojahed, Master thesis, NTNU, Trondheim (unpublished) (2020)